# Upper Particle Size Limit for High-Speed Analysis by Sedimentation/Steric Field-Flow Fractionation in Thin Channels

**Myeong Hee Moon[†] and J. Calvin Giddings*[,‡]**

*Field-Flow Fractionation Research Center, Department of Chemistry, University of Utah, Salt Lake City, Utah 84112*

This work describes some of the limitations encountered when sedimentation/steric field-flow fractionation is used to separate and analyze particles whose diameters approach a substantial fraction of the thickness of the FFF channel. Results obtained for a thin (127 $\mu$m thick) channel indicate a departure from linear calibration for particle diameters that approach 25−30% of the channel thickness and a substantial loss of selectivity for diameters at 50% of the channel thickness. These results are explained by a simple theoretical model. In addition, our measurements show that the larger particles (in this case polystyrene latex beads of 60 $\mu$m diameter) are subject to peak distortion and sample loss unless high flowrates and low field strengths are employed.

The capability of field-flow fractionation (FFF) techniques to separate and characterize macromolecules and particles has been widely demonstrated (Giddings, 1993a; Weers and Arlauskas, 1995; van Asten et al., 1995; Blanda et al., 1994; Levin et al., 1994; Schimpf et al., 1993; Beckett and Hart, 1993; Caldwell and Gao, 1993). The FFF techniques are especially effective for particles and can be used over a particle size range that extends 5 orders of magnitude from about 1 nm to 100 $\mu$m. FFF not only can achieve separation across this substantial size range but also is capable of yielding measurements of the physical properties (mass, hydrodynamic diameter, density, etc.) of the separated constituents (Giddings, 1993a; Giddings, 1995). Since FFF is an elution separation method, it has the additional advantage that particle fractions can be collected for further examination and characterization by electron microscopy, light scattering, and techniques used for elemental analysis such as ICP-MS (Giddings, 1995; Taylor et al., 1992; Caldwell et al., 1992).

The large particle size range to which FFF is applicable divides naturally into two parts subject to two different FFF retention mechanisms. The so-called normal mode (or Brownian mode) of FFF is applicable across the submicron size range. Above ~1 $\mu$m, the steric (or lift-hyperlayer) mode, entailing a different separation mechanism (see Figure 1), is applicable. (If conditions are carefully chosen, steric FFF is applicable down to 0.3 $\mu$m (Moon and Giddings, 1992).) For normal-mode FFF, retention time increases with particle size. For steric FFF, retention time decreases with increasing particle diameter. The steric transition region is that part of the particle diameter range where the two mechanisms contribute about equally to retention. The mechanism of the steric transition and of the two underlying modes of FFF operation has been detailed in the literature (Moon and Giddings, 1992; Giddings, 1993b).

Different forces can be used to drive the FFF process, depending upon the requirements of separation. For the analysis of both colloidal and larger sized particles, sedimentation forces (generated by a centrifuge) have proved very effective, yielding high selectivities and high resolution. This investigation is focused on the use of sedimentation forces to separate larger particles (>1 $\mu$m) in the steric mode of FFF; the resulting subtechnique is called sedimentation/steric FFF or Sd/StFFF. Here we propose to examine the upper size limit of particles that can be successfully separated by Sd/StFFF in channels that are thinner than conventional channels.

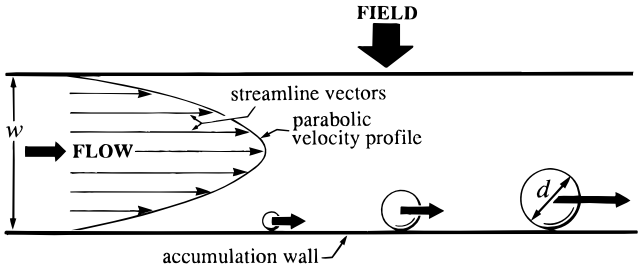


**Figure 1.** Mechanism of differential migration and separation of particles by steric FFF.

The means by which Sd/StFFF achieves separation is shown in Figure 1, which provides a simplified view of the steric separation mechanism. All particles in the steric size range ($d > 1$ $\mu$m) are driven to the accumulation wall by the applied field. They are subsequently driven along the channel axis by laminar flow. Larger particles, which extend further toward the center of the parabolic velocity profile, are displaced at a higher velocity than the smaller particles which are confined near the wall. Because the different sizes have different displacement velocities, they elute from the FFF channel at different times. (Because of hydrodynamic lift forces, the particles are actually elevated slightly above the accumulation wall and thus do not normally make direct contact with the wall.)

Sd/StFFF, particularly when carried out in thin channels, is capable of separating supramicron-sized particles with both high resolution and high speed. This is illustrated in Figure 2 which shows a fractogram (signal-versus-time curve) for the separation of polystyrene latex beads ranging from 4 to 48 $\mu$m in diameter using Sd/StFFF in a 127 $\mu$m thick channel. The separation time for the seven different sizes of latexes is only 3.5 min. The combination of high resolution and

* Author to whom correspondence should be addressed.
[†] Present address: Department of Chemistry, Kangnung National University, Jibyun-Dong San-1, Kangnung, Kangwon-do, Korea.
[‡] Phone: 801-581-6683. Fax: 801-581-4353. E-mail: Giddings@chemistry.chem.utah.edu.

0888-5885/96/2635-1072$12.00/0 

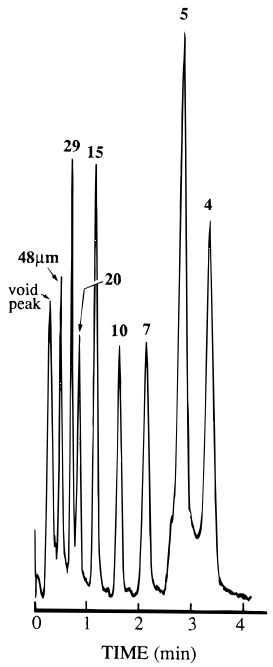


**Figure 2.** Sedimentation/steric FFF fractogram showing high-speed separation of polystyrene latex beads of the indicated diameters in a thin ($w$ = 127 $\mu$m) channel. The flowrate is 6.01 mL/min and the rotation rate 1300 rpm.

high speed with system flexibility has made Sd/StFFF (and related steric FFF methods) an attractive tool for the analysis of biological cells, environmental sediments, chromatographic supports, and numerous industrial materials (Moon and Giddings, 1992; Giddings, 1993b; Ratanathanawongs and Giddings, 1994; Beckett et al., 1994; Cardot et al., 1994; Yue et al., 1994; Pazourek et al., 1994; Barman, 1994; Moon and Giddings, 1993; Barman et al., 1993; Giddings and Moon, 1991; Giddings et al., 1991a).

The ribbon-shaped channels that have traditionally been used in sedimentation FFF are 254 $\mu$m (0.01 in.) thick. In recent work we have utilized thinner channels, in most cases with a thickness $w$ of 127 $\mu$m (Moon and Giddings, 1992, 1993; Giddings and Moon, 1991). The thinner channels have several advantages: one can generally achieve higher speeds, stronger detector signals, better recoveries, and faster relaxation and operate at lower flowrates (Giddings et al., 1991c). The latter point is important in Sd/StFFF where flowrates above 10 mL/min are generally required for reasonably fast analysis. (The separation shown in Figure 2 required a flowrate of only 6 mL/min.) However, the thinner channels have the disadvantage that the particle size range subject to separation is reduced. This reduction in range occurs at both the lower and upper particle diameter limits of sedimentation FFF. This study is concerned only with the upper particle diameter limit of thin channels.

One absolute constraint that limits the maximum particle size is apparent. Clearly, FFF is incapable of eluting any particle whose diameter $d$ exceeds channel thickness $w$ because it would be physically impossible for particles with $d > w$ to fit within the confines of the channel. However, the practical upper limit of $d$ is considerably smaller than this geometrical constraint would imply. One expects a loss of selectivity (see below) for particles with $d$ approaching $w$. In addition, we observe problems with particle recovery for larger $d$'s in this study. These matters are described below.

## Theoretical Considerations

In Sd/StFFF (along with other forms of steric and lift-hyperlayer FFF), the equilibrium position of a particle in the FFF channel is determined by the balance between the driving force and the opposing hydrodynamic lift forces. The hydrodynamic lift forces have been studied using Sd/StFFF and have been found to be exceedingly complicated (Williams et al., 1992a, 1994, 1996). Consequently, particle size analysis is generally carried out using an empirical calibration procedure.

Calibration is based on the observation that, if the logarithm of retention time $t_r$ is plotted against the logarithm of particle diameter $d$, a straight line is produced over a considerable size range (Giddings et al., 1991b). Departures from the straight line plot occur at the lower end at about $d = 1$ $\mu$m due to the steric transition and the increasing dominance of normal-mode retention for smaller particles (Moon and Giddings, 1992; Giddings, 1993b). The upper size limit to which the straight-line calibration procedure applies has not been established. However, some approximate theoretical guidelines can be used to suggest the basis and approximate location for a significant departure from straight-line calibration for larger particles.

The straight-line (or linear) calibration is described by the relationship

$$\log t_r = \log t_{r1} - S_d \log d \qquad (1)$$

where $t_{r1}$ and $S_d$ are calibration constants. These constants are generally obtained from a calibration run (resembling that shown in Figure 2) using polystyrene latex beads as size standards. The use of these constants to describe the $t_r - d$ relationship for an uncharacterized particulate material requires that both the flowrate and the product ($G\Delta\rho$) be the same in the calibration run and the sample run. The requirement for a constant $G\Delta\rho$ appears restrictive, but it is not: the operator can adjust field strength $G$ to accommodate sample particles of different densities $\rho_p$ and thus different increments $\Delta\rho$ in density between the sample particles and the carrier solution. The adjustment in $G$ to allow for differences in $\Delta\rho$ is termed the density compensation method for calibration (Giddings et al., 1991b).

The calibration constant $S_d$ is equivalent to the diameter selectivity defined by

$$S_d = \left| \frac{\mathrm{d} \log t_r}{\mathrm{d} \log d} \right| \qquad (2)$$

Values of $S_d$ typically lie in the range 0.7−0.8.

A simple model of steric FFF explains the basis of both the linear calibration as described by eq 1 and the observed departures from linear calibration. However, the complications of lift forces and the retardation effect, a hydrodynamic effect leading to the reduction of particle velocity (Williams et al., 1992a, 1994), are ignored in this model. The simple model (see Figure 1) envisions the particles being displaced along the channel accumulation wall at a velocity equal to the streamline velocity at the particle center, which is assumed to be located one radius ($d$/2) from the channel wall (Giddings and Myers, 1978). Because the flow profiles are parabolic, this model suggests that the velocity $v_p$ of displacement of a particle down the channel is related to its diameter $d$ by

$$v_p = 3\langle v\rangle\left(\frac{d}{w} - \frac{d^2}{2w^2}\right) \quad (3)$$

where $\langle v\rangle$ is the mean cross-sectional flow velocity. We note that the velocity ratio $v_p/\langle v\rangle$, equal to the retention ratio $R$, is equal to the time ratio $t^0/t_r$, where $t^0$ is the void time or, equivalently, the elution time of a nonretained component. Consequently, $t_r$ is approximated by

$$t_r = \frac{t^0}{\frac{3d}{w}\left(1 - \frac{d}{2w}\right)} \quad (4)$$

The logarithmic form of this equation is

$$\log t_r = \log(t^0/3) - \log(d/w) - \log(1 - d/2w) \quad (5)$$

The first two terms on the right-hand side of this equation provide the same log linear relationship as eq 1 except that $S_d$ is required by eq 5 to be unity, whereas in usual practice $S_d < 1$ as noted above. The final term of eq 5 is negligible for $d/w << 1$ but makes an increasingly positive contribution to log $t_r$ with increasing $d/w$. Thus, this model predicts a loss in selectivity $S_d$ with increasing $d$ and suggests that larger particles will have retention times in excess of those predicted by a linear log−log plot. In other words, the elution of larger particles, where $d$ approaches $w$, will lag behind that predicted by normal calibration. This departure from linear calibration can be traced back to the second-order term in the parabolic flow expression of eq 3.

While the model leading to eq 5 is too oversimplified for quantitative use, it shows the basis for expecting a log linear relationship for $d/w << 1$ and, furthermore, for expecting departures from this straight-line relationship (with an attendant loss in selectivity) when $d$ increases to become a significant fraction of channel thickness $w$. The model also suggests that departures from linearity are not a function of $d$ alone but of the dimensionless ratio $d/w$; it further suggests that a universal calibration curve might result using a log−log plot of the dimensionless parameters $t_r/t^0$ and $d/w$. (Further work would be required to determine the changes in field strength and shear rate needed to make such a universal plot valid for different values of $w$.) While the model could be further improved (e.g., by setting $v_p$ equal to the average velocity of undisturbed streamlines intercepting the particle cross section normal to flow), useful quantitative results from the model are not expected without accounting for the complicated hydrodynamic effects noted earlier (Williams et al., 1992b). The main purpose of the model is to provide guidance in the interpretation of experimental results.

## Experimental Section

Separation was carried out using a sedimentation FFF system with the same basic structure and operational parameters as the Model S101 Colloid/Particle Fractionator from FFFractionation (Salt Lake City, UT). A polished Hastelloy-C alloy was used for the channel walls. The channel in this system has a length of 90.0 cm, a breadth of 1.0 cm, and a thickness $w$ of 0.0127 cm. The channel void volume measured as a nonretained peak of sodium benzoate was 1.18 mL, excluding the dead volume leading to the detector from the channel outlet.

The particle standards used for this study were polystyrene latex beads (density 1.053 g/cm$^3$) from Duke Scientific (Palo Alto, CA) with nominal diameters of 3.97, 5.002, 7.04, 9.87, 15.0, 20.54, 29.4, 47.9, and 59.7 $\mu$m (hereafter they are referred to as 4, 5, 7, 10, 15, 21, 29, 48, and 60 $\mu$m particles, respectively). The carrier liquid (density 0.997 g/cm$^3$) consisted of doubly distilled water with 0.1% FL-70 (Fisher Scientific, Fairlawn, NJ) added as a mixed anionic−nonionic surfactant to aid dispersion of the polystyrene particles and 0.02% sodium azide added as a bactericide. A Kontron LC pump (Kontron Electrolab, London, U.K.) was used for fluid delivery to the FFF channel. Another pump, an FMI Lab pump (Model QD-2 (Fluid Metering, Inc., Oysterbay, NY) was utilized for flushing the channel at high speed (about 30 mL/min) after each sample run to remove any debris accumulated on the channel surface. The eluted sample particles at the outlet of the channel were monitored at 300 nm by a Spectroflow Monitor SF770 UV−vis detector (Kratos Analytical Instruments, Westwood, NJ). A strip chart recorder (Houston Instrument Corp., Austin, TX) was used for recording the detector response.

All samples except the 60 $\mu$m latex were injected directly onto the channel using a microsyringe and a septum injection device. Once injected, channel rotation was started. After the 1−2 min required to reach the desired rotation rate, channel flow was initiated. (This period of rpm startup also served as a stop-flow time for sample relaxation.) In contrast to the other samples, the 60 $\mu$m latex was injected directly into the flowstream entering the channel via the rotating seal. In this case, the channel was rotating at full speed prior to injection. No stop-flow procedure was used because of the rapid relaxation of such large latex particles. All latex standards were injected directly without dilution or sonication; the injection volumes were generally 1−2 $\mu$L for each standard.

## Results and Discussion

A series of calibration plots were reported in an earlier publication based on retention measurements for a 254 $\mu$m thick FFF channel (Giddings et al., 1991b). The calibration plots remained linear, in accordance with eq 1, for latex particle diameters as large as 48 and 60 $\mu$m, with only a very slight departure observed for the 60 $\mu$m latex. In order to compare the linearity of calibration with that observed for the thin (127 $\mu$m thick) channel, we have constructed calibration plots at four different values of field strength or rotational speed (rpm). These four calibration plots, along with a plot based on the simplified theoretical model, are shown in Figure 3. The four plots differ from one another because of lift forces. The upward curvature of the experimental plots for the largest two particle diameters (48 and 60 $\mu$m) is apparent from the figure. Linearity does not appear to be valid much beyond the size of the third largest particle, $d$ = 30 $\mu$m. However, more closely spaced sizes would need to be examined to fill in the details of the initial departure from linearity.

While the observed departure from linearity complicates calibration, it does not eliminate the possibility of calibration. However, in the present case, the nonlinearity is associated with a reduction in the absolute value of the slope of the calibration plot, which represents a reduction in selectivity (see eq 2).

From the results shown in Figure 3, the simple theoretical model appears to be validated for its predic-

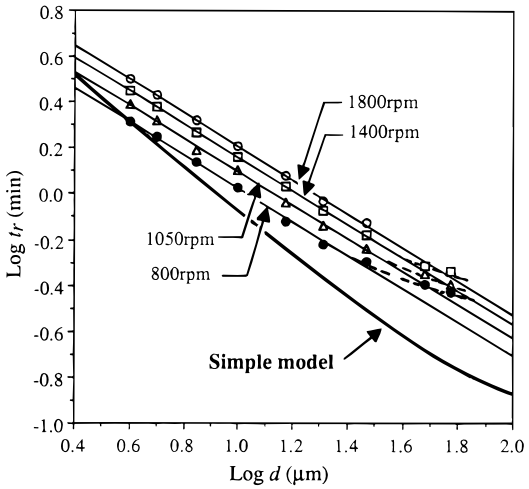


**Figure 3.** Calibration plots obtained using polystyrene latex beads at a flowrate of 6.15 mL/min and at four different rotation rates. Results of the simple model are shown for comparison.

**Table 1. Experimental Conditions and Parameters Corresponding to the Calibration Plots of Figure 2 (All Flowrates are 6.15 mL/min)**

| plot | rpm | $G\Delta\rho \times 10^{-4}$ (g/s$^2$ cm$^2$) | $S_d$ | $t_{r1}$ (min) | cc[a] |
|---|---|---|---|---|---|
| a | 1800 | 2.68 | 0.735 | 8.78 | 0.999 |
| b | 1400 | 1.62 | 0.727 | 7.70 | 1.000 |
| c | 1050 | 0.913 | 0.722 | 6.55 | 0.999 |
| d | 800 | 0.530 | 0.728 | 5.64 | 0.997 |

[a] Correlation coefficient for plot.

tion of (a) upward curvature or nonlinearity and, as a consequence, a loss of selectivity for larger $d$ values and (b) the relatively early onset of nonlinearity in thin FFF channels. The numerical agreement between experimental and predicted plots is poor, as expected.

The four straight calibration lines shown in Figure 3 were obtained by a least-squares fit of data for particles up to 30 $\mu$m diameter to the calibration expression given by eq 1. The two calibration parameters ($S_d$ and $t_{r1}$) and other relevant data are given in Table 1.

A second significant phenomenon observed in this work, aside from nonlinear calibration, is the distortion and disappearance of particle peaks under some experimental conditions. It is important to determine the circumstances of this peak distortion/loss in order to avoid its effects in practical applications.

We note first that two points are missing in Figure 3 for the two largest particles (48 and 60 $\mu$m) at the highest field strength (1800 rpm). Their absence is a consequence of peak distortion and loss. In general, this phenomenon appears to be associated with relatively large $d$ values, high field strengths, and low flowrates.

The effect of flowrate is illustrated in Figure 4. Here fractograms are shown for three runs at 960 rpm at three different flow velocities using only 60 $\mu$m latex beads. In principle, the peak height should remain approximately constant and the peak area should increase in inverse proportion to flowrate. The significant reduction in peak height observed with decreasing flowrate suggests a loss of sample material. Furthermore, the peak is substantially distorted at the lowest flowrate, with a tendency toward peak splitting and the formation of a double peak.

Figure 5 shows the results of experiments carried out at a higher field strength: 1200 rpm (243.7$g$) compared to 960 rpm (155.7$g$) for Figure 4. At the higher flowrate

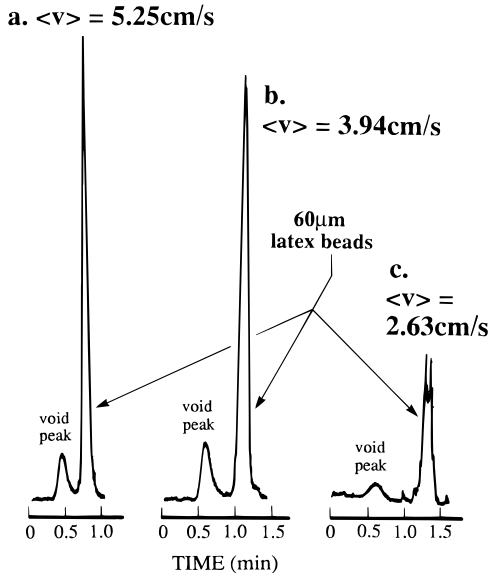


**Figure 4.** Fractogram for 60 $\mu$m latex particles obtained at 960 rpm using the different flow velocities indicated. Stopless flow injection was used.

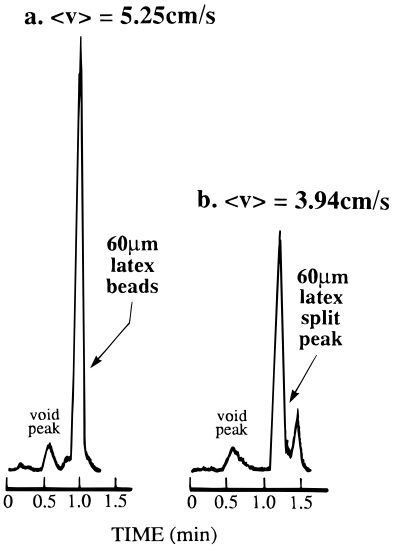


**Figure 5.** Fractogram for a 60 $\mu$m latex obtained at 1200 rpm using stopless flow injection.

of $\langle v \rangle$ = 5.25 cm/s the peak is sharp and well formed, with about 98% of the area of the comparable peak in Figure 4. However, at $\langle v \rangle$ = 3.94 cm/s, the peak is badly split and has reduced area. Note that this flow velocity is sufficient to produce an excellent peak at 960 rpm (Figure 4).

The negative effect of excessively high field strengths is further emphasized in Figure 6, which reports fractograms of the 60 $\mu$m latex obtained at 1400 rpm (331.2$g$). At this field strength, the previous satisfactory flow velocity of $\langle v \rangle$ = 5.25 cm/s now produces a double peak of reduced area. It is necessary to increase $\langle v \rangle$ to 6.56 cm/s to produce a sharp undistorted peak.

Figures 4−6 clearly demonstrate the deleterious effect of high field strength combined with low flowrates on peak distortion and loss for large particles. Additional experiments show a systematic trend as these two parameters move into an unfavorable range. Concurrent with the loss of peak area, a small satellite peak appears following the main peak. With further increases/decreases in field strength/flowrate, the satellite peak

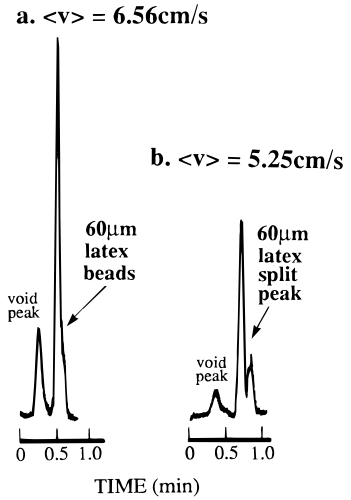


**Figure 6.** Elution profiles for 60 $\mu$m latex particles obtained at 1400 rpm.

grows in relative area, broadens, and eventually disappears along with the main peak.

The above observations regarding peak distortion and loss appear to be consistent with the occurrence of particle-wall adhesion modulated by hydrodynamic lift forces. Any tendency toward adhesion, particularly if it involves short-range forces, would be opposed by lift forces, which drive particles away from the wall. These lift forces increase with flow velocity (shear rate), thus explaining the beneficial effect of increased flowrate in reducing peak distortion and loss. However, lift forces can be offset by a high field strength, which drives particles closer to the wall and makes them more susceptible to adhesion forces. Unfortunately, a better understanding of lift forces is needed in order to translate this mechanism into practical guidelines for avoiding the negative effects described above.

## Conclusions

This work demonstrates some of the constraints that must be considered when Sd/StFFF is used for the separation and analysis of particles whose size approaches a substantial fraction of the thickness of the FFF channel. We have found, first of all, that linear calibration is applicable only for $d/w$ ratios that lie below 0.25 or, at most, 0.3. Larger particles, with $d/w$ ratios approaching 0.5, can be separated but care must be taken to use sufficiently high flowrates and mild field strengths to avoid peak distortion and sample loss. However, for larger particles with $d/w$ ratios approaching 0.5, selectivity is substantially diminished, as indicated by the reduced absolute slopes of the calibration plots.

It is important to note that the above constraints have been established only for thin channels (in the present case $w = 127$ $\mu$m) and do not impose any ceiling on the largest particle diameter separable by Sd/StFFF in channels of arbitrary thickness. To the contrary, our results show only that $d$ is constrained to some fraction (about 0.5) of channel thickness $w$, which suggests that very large particles could be separated in thick channels. This observation is supported by previous work done in this laboratory in which particles up to 500 $\mu$m diameter were separated in a 1 mm thick channel (Liu, 1992). It is likely that much larger particles still could be separated. The primary constraint to absolute particle size is likely to be a hydrodynamic one, involving the necessity of generating sufficiently high shear rates to keep large particles mobilized. This topic will be discussed in a forthcoming publication.

An essential element in understanding and quantitatively describing upper particle diameter limits is an improved theoretical foundation for hydrodynamic lift forces. These forces influence the position and shape of the calibration plots and determine the linear range of such plots. Hydrodynamic lift forces, by keeping particles elevated above the channel wall, also combat the negative effects of particle-wall adhesion. Sd/StFFF can serve as a highly effective tool for the measurement of lift forces; results so far show that much work is still needed to characterize these important forces (Williams et al., 1992a, 1994, 1996).

## Acknowledgment

This work was supported by Grant CHE-9322472 from the National Science Foundation.

## Nomenclature

$d$ = particle diameter
$G$ = field strength measured as acceleration
$R$ = retention ratio
$S_d$ = calibration constant; diameter-based selectivity
$t^0$ = void time
$t_r$ = retention time
$t_{r1}$ = calibration constant; $t_r$ for particle of unit diameter
$\langle v \rangle$ = mean cross sectional flow velocity
$v_p$ = particle velocity
$w$ = channel thickness

*Greek Letters*

$\Delta\rho$ = density difference between particle and carrier liquid
$\rho_p$ = particle density

## Literature Cited

Barman, B. N. Monitoring of the Dispersion of Aggregated Red Blood Cells by Flow/Hyperlayer Field-Flow Fractionation. *J. Colloid Interface Sci.* **1994**, *167*, 467.

Barman, B. N.; Ashwood, E. R.; Giddings, J. C. Separation and Size Distribution of Red Blood Cells of Diverse Size, Shape, and Origin by Flow/Hyperlayer Field-Flow Fractionation. *Anal. Biochem.* **1993**, *212*, 35.

Beckett, R.; Hart, B. T. Use of Field-Flow Fractionation Techniques to Characterize Aquatic Particles, Colloids and Macromolecules. In *Environmental Particles*; Buffle, J.; van Leeuwen, H. P., Eds.; CRC Press: Boca Raton, FL, 1993; Vol. 2, pp 165−205.

Beckett, R.; Jiang, Y.; Liu, G.; Moon, M. H.; Giddings, J. C. Separation and Behavior of Nonspherical Particles in Sedimentation/Steric Field-Flow Fractionation. *Part. Sci. Technol.* **1994**, *12*, 89−113.

Blanda, M.; Reschiglian, P.; Dondi, F.; Beckett, R. Characterization of Low-Density Polybutadiene Latexes by Sedimentation Field-Flow Fractionation. *Polym. Int.* **1994**, *33*, 61.

Caldwell, K. D.; Gao, Y.-S. Electrical Field-Flow Fractionation in Particle Separation. 1. Monodisperse Standards. *Anal. Chem.* **1993**, *65*, 1764.

Caldwell, K. D.; Li, J.; Li, J.-T.; Dalgleish, D. G. Adsorption Behavior of Milk Proteins on Polystyrene Latex. A Study Based on Sedimentation Field-Flow Fractionation and Dynamic Light Scattering. *J. Chromatogr.* **1992**, *604*, 63.

Cardot, Ph. J. P.; Elgéa, C.; Guernet, M.; Godet, D.; Andreux, J. P. Size- and Density-Dependent Elution of Normal and Pathological Red Blood Cells by Gravitational Field-Flow Fractionation. *J. Chromatogr. B* **1994**, *654*, 193.

Giddings, J. C. Field-Flow Fractionation: Separation and Characterization of Macromolecular, Colloidal, and Particulate Materials. *Science* **1993a**, *260*, 1456.

Giddings, J. C. Retention (Steric) Inversion in Field-Flow Fractionation: Practical Implications in Particle Size, Density, and Shape Analysis. *Analyst* **1993b**, *118*, 1487.

Giddings, J. C. Measuring of Colloidal and Macromolecular Properties by FFF. *Anal. Chem*. **1995**, *67*, 592A.

Giddings, J. C.; Myers, M. N. Steric Field-Flow Fractionation: A New Method for Separating 1−100 $\mu$m Particles. *Sep. Sci. Technol*. **1978**, *13*, 637.

Giddings, J. C.; Moon, M. H. Measurement of Particle Density, Porosity, and Size Distributions by Sedimentation/Steric Field-Flow Fractionation: Application to Chromatographic Supports. *Anal. Chem*. **1991**, *63*, 2869.

Giddings, J. C.; Barman, B. N.; Liu, M.-K. Separation of Cells by Field-Flow Fractionation and Related Methods. In *Cell Separation Science and Technology*; Kompala, D. S.; Todd, P., Eds.; ACS Symposium Series 464; American Chemical Society: Washington, DC, 1991a; pp 128−144.

Giddings, J. C.; Moon, M. H.; Williams, P. S.; Myers, M. N. Particle Size Distribution by Sedimentation/Steric FFF: Development of a Calibration Procedure Based on Density Compensation. *Anal. Chem*. **1991b**, *63*, 1366.

Giddings, J. C.; Ratanathanawongs, S. K.; Moon, M. H. Field-Flow Fractionation: A Versatile Technology for Particle Characterization in the Size Range $10^{-3}$ to $10^{2}$ Micrometers. *Kona: Powder Particle* **1991c**, *9*, 200.

Levin, S.; Stern, L.; Ze'evi, A.; Levy, M. Y. Characterization of Submicrometer Emulsions Using Sedimentation Field-Flow Fractionation with Power Field Programming. *Anal. Chem*. **1994**, *66*, 368−377.

Liu, G. Separation and Characterization of Particles by Field-Flow Fractionation. Ph.D. Thesis, University of Utah, Salt Lake City, UT, Dec 1992.

Moon, M. H.; Giddings, J. C. Extension of Sedimentation/Steric Field-Flow Fractionation into Submicron Range: Size Analysis of 0.2−15 $\mu$m Metal Particles. *Anal. Chem*. **1992**, *64*, 3029.

Moon, M. H.; Giddings, J. C. Rapid Separation and Measurement of Particle Size Distribution of Starch Granules by Sedimentation/Steric Field-Flow Fractionation. *J. Food Sci*. **1993**, *58*, 1166.

Pazourek, J.; Urbánková, E.; Chmelík, J. Experimental Study on the Separation of Silica Gel Supports by Gravitational Field-Flow Fractionation. *J. Chromatogr. A* **1994**, *660*, 113.

Ratanathanawongs, S. K.; Giddings, J. C. Rapid Size Characterization of Chromatographic Silicas by Flow Field-Flow Fractionation. *Chromatographia* **1994**, *38*, 545.

Schimpf, M. E.; Rue, C.; Mercer, G.; Wheeler, L. M.; Romeo, P. F. Studies in the Thermal Diffusion of Copolymers Using Field-Flow Fractionation. *J. Coatings Technol*. **1993**, *65*, 51−56.

Taylor, H. E.; Garbarino, J. R.; Murphy, D. M.; Beckett, R. Inductively Coupled-Plasma-Mass Spectrometry as an Element-Specific Detector for Field-Flow Fractionation Particle Separation. *Anal. Chem*. **1992**, *64*, 2036.

van Asten, A. C.; Kok, W. Th.; Tijssen, R.; Poppe, H. Thermal Field-Flow Fractionation of Polytetrahydrofuran. *J. Chromatogr*. **1994**, *676*, 361.

Weers, J. G.; Arlauskas, R. A. Sedimentation Field-Flow Fractionation Studies of Ostwald Ripening in Fluorocarbon Emulsions Containing Two Disperse Phase Components. *Langmuir* **1995**, *11*, 474−477.

Williams, P. S.; Koch, T.; Giddings, J. C. Characterization of Near-Wall Hydrodynamic Lift Forces Using Sedimentation Field-Flow Fractionation. *Chem. Eng. Commun*. **1992a**, *111*, 121.

Williams, P. S.; Moon, M. H.; Giddings, J. C. Fast Separation and Characterization of Micron Size Particles by Sedimentation/Steric Field-Flow Fractionation: Role of Lift Forces. In *Particle Size Analysis*; Stanley-Wood, N. G.; Lines, R. W., Eds.; Royal Society of Chemistry: Cambridge, UK, 1992b; pp 280−289.

Williams, P. S.; Lee, S.; Giddings, J. C. Characterization of Hydrodynamic Lift Forces by Field-Flow Fractionation. Inertial and Near-Wall Lift Forces. *Chem. Eng. Commun*. **1994**, *130*, 143.

Williams, P. S.; Moon, M. H.; Xu, Y.; Giddings, J. C. Effect of Viscosity on Retention Time and Hydrodynamic Lift Forces in Sedimentation/Steric Field-Flow Fractionation. *Chem. Eng. Sci*. **1996**, submitted.

Yue, V.; Kowal, R.; Neargarder, L.; Bond, L.; Muetterties, A.; Parsons, R. Miniature Field-Flow Fractionation System for Analysis of Blood Cells. *Clin. Chem*. **1994**, *40*, 1810.

*Received for review* June 1, 1995
*Revised manuscript received* September 8, 1995
*Accepted* September 19, 1995[⊗]

IE9503297

[⊗] Abstract published in *Advance ACS Abstracts*, February 15, 1996.